ELSEVIER

Contents lists available at ScienceDirect

Biosensors and Bioelectronics

journal homepage: http://www.elsevier.com/locate/bios





Nanosensors for single cell mechanical interrogation

Xinxin Hang ^{a,1}, Shiqi He ^{a,1}, Zaizai Dong ^a, Grayson Minnick ^b, Jordan Rosenbohm ^b, Zhou Chen ^{d,**}, Ruiguo Yang ^{b,c,***}, Lingqian Chang ^{a,*}

- ^a Beijing Advanced Innovation Center for Biomedical Engineering, School of Biological Science and Medical Engineering, Beihang University, No.37, Xueyuan Road, Haidian District, Beijing, 100191, China
- b Department of Mechanical and Materials Engineering, University of Nebraska-Lincoln, Lincoln, NE, 68588, USA
- ^c Nebraska Center for Integrated Biomolecular Communication, University of Nebraska-Lincoln, Lincoln, NE, 68588, USA
- ^d School of Mechanical and Power Engineering, Nanjing Tech University, Nanjing, 211800, China

ARTICLE INFO

Keywords: Cell mechanics Force sensors FRET Tension gauge tether DNA hairpin

ABSTRACT

The occurrence and development of many diseases are accompanied and sometimes dictated by the destruction of biomechanical homeostasis. For instance, cancer cells and normal cells show different cellular mechanical forces phenotypes, as the proliferation and invasion ability of cancer cells is often related to the changes in mechanical force in the tumor. With single cell analysis, variations in mechanics within a cell population can be detected and analyzed, opening new dimensions in the study of cancer. Nanosensor design for interrogation of cell mechanics is an interdisciplinary area bridging over cell biology, mechanics, and micro/nanotechnology. In this tutorial review, we give insight into the background and technical innovation of currently available methods for mechanical analysis of cells. First, we discuss the mechanism of mechanical changes in the development and progression of cancer that shows the feasibility of mechanical sensors in cancer cell detection. Next, we summarize the principle, progress, and essential problems of common technologies for cell force measurement, including single molecule force spectroscopy and elastic substrate-sensors. Following that, we discuss novel micro and nano-scale mechanical sensors and their applications in single cell level biological analysis. At last, we elaborate on the remaining issues and trends of the cellular mechanical sensors.

1. Introduction

Cells not only generate internal forces but also respond to external forces. The routine functions of living cells, including differentiation, division, migration, and apoptosis, are dynamically orchestrated by mechanical signals (Jheng et al., 2018; Pinto et al., 2014; Carlton et al., 2020). The balance between the input and output of the mechanical signals essentially dictates cellular homeostasis. Once stability is disturbed, cells may undergo functional disorders in growth and development, and even genetic alterations (Kai et al., 2016; Shi et al., 2015). Last several years, multiple efforts have been made to gain a deeper understanding of the mechanical properties of cells exposed to stress and strain generated locally by cell-cell interaction and cellular microenvironments, including activation of mechanosensitive ion

channels, focal adhesion response to matrix stiffness and cell-cell junction response to mechanical tension between neighboring cells (Kobayashi and Sokabe, 2010; Geiger et al., 2009, Han and Rooij, 2016). As one of the significant signals regulating cell fate, guiding tissue development, and postpartum functions, cellular forces were rarely investigated in a quantitative way until recent decades when atomic force microscopy (AFM), optical tweezers (OT), magnetic tweezers (MT), and traction force microscopy (TFM) provided a reliable mehod for cell mechanics research (Fig. 1). For instance, AFM can probe the cell membrane and produce apparent stiffness values from force-distance curves which reveal the molecular activities and heterogeneities of cells (Li et al., 2017b; Carvalho et al., 2010; Dupres et al., 2009; Guedes et al., 2016). Additionally, OT and MT have been widely used to study the mechanical behavior of cell cytoskeleton (Mandal et al., 2016;

^{*} Corresponding author. Beijing Advanced Innovation Center for Biomedical Engineering, School of Biological Science and Medical Engineering, Beihang University, No.37, Xueyuan Road, Haidian District, Beijing, 100191, China.

^{**} Corresponding author. School of Mechanical and Power Engineering, Nanjing Tech University, Nanjing, 211800, China.

^{***} Corresponding author. Department of Mechanical and Materials Engineering, University of Nebraska-Lincoln, Lincoln, NE, 68588, USA. E-mail addresses: zchen6240@njtech.edu.cn (Z. Chen), ryang6@unl.edu (R. Yang), lingqianchang@buaa.edu.cn (L. Chang).

 $^{^{1}\,}$ These authors contribute equally to the work.

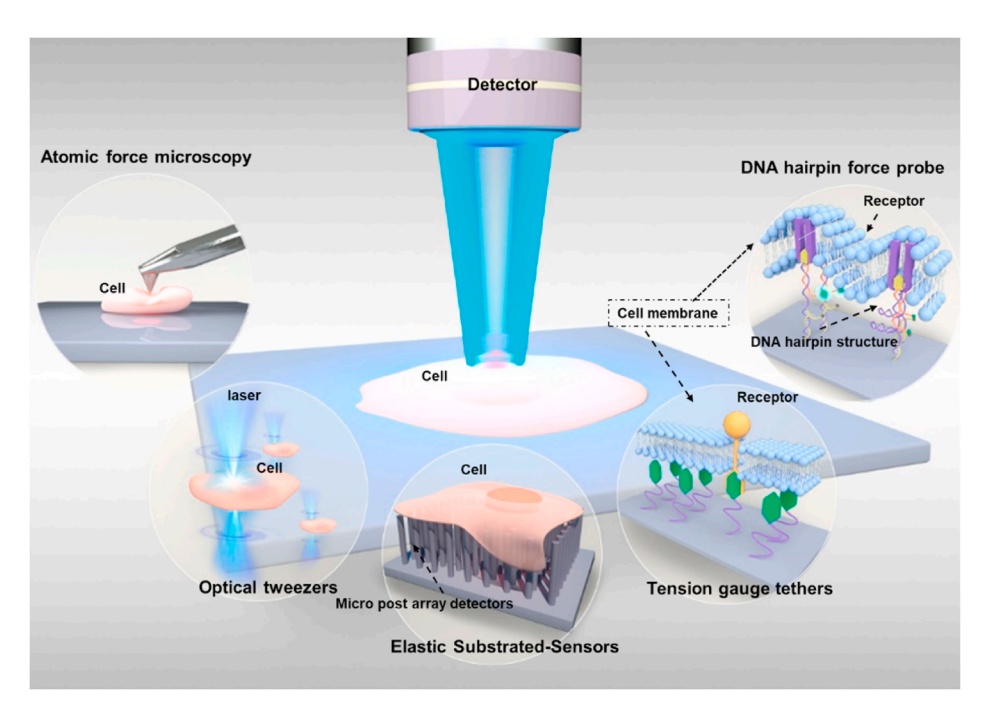


Fig. 1. The available platforms for cellular mechanical measurement summarized in this review. Among them, AFM, OT and elastic substrate-sensors reflect the changes of cell mechanical force by measuring ECM stiffness and Young's modulus (Section 3). TGT and DNA hairpin force probes based on FRET to detect the mechanical force distribution on the cell surface (Section 4).

Schwingel and Bastmeyer, 2013; Wang et al., 1993; Matthews et al., 2006). Lastly, for its ease of use in measuring cell-extracellular matrix (ECM) adhesion, TFM has been demonstrated as an effective way to study cell proliferation, migration, and differentiation (Ma and Salaita, 2019; Banda et al., 2019; Rauskolb et al., 2014; Reilly and Engler, 2010). An entire new group of force sensors were recently developed to study intracellular tension at the molecular level. For example, the Förster resonance energy transfer (FRET)-based tension sensors have allowed the analysis of mechanical processes with piconewton (pN) sensitivity in cells (Freikamp et al., 2016; Cost et al., 2015; Eder et al., 2017). Furthermore, DNA-based force sensors, as a novel molecular tension sensor, have shown advantages in cell mechanics research due to their superior force sensitivity, temporal/spatial resolution, and high throughput (Liu et al., 2017). These interactions with forces at the pN-level are more meaningful to explore at the single cell level.

In this review, we summarize the general design principles of the recently developed novel micro and nano-sensors for measuring mechanical properties of cells. We first summarize the principles, progress, and essential problems of the two common types of cellular force measurement tools (single molecule force spectroscopy, SMFS and elastic substrate sensors). We then describe two new types of devices (tension gauge tethers, TGT and DNA hairpin force probe), which have higher force resolution and throughput than traditional devices. At last, we shed light on the research trends of the cellular mechanical sensors for the future.

2. Mechanical heterogeneities

Mechanical forces are continuously and dynamically generated in cell-cell and cellular ECM interactions. Regarding the mechanical properties of cancer, it is generally characterized as a palpable 'stiffening' of the tissue due to compromised tensional homeostasis. Furthermore, the presence of desmoplastic stroma makes many solid tumors significantly stiffer than normal tissues (Butcher and Weaver, 2009; Levental et al., 2009; Watson, 2006; Holmbeck and Szabova, 2010). Cancers are usually associated with fibrosis, usually showing increased resident cell motility associated with pathology and

accompanied by an invasion of foreign cells (Lu et al., 2011; Kothapalli et al., 2012). For example, the increases in breast density and collagen content may be the results of increased deposition, decreased reshaping, or increased post-translational modification (e.g., cross-linking of specific ECM components). A variety of collagens show increased deposition during tumor formation (e.g., Collagen Type I, II, III, V, and IX) (Barsky et al. 1982). This phenotype characterized by a profound pro-proliferative response is particularly evident in human breast cancer, which accompanied by more significant ECM remodeling and crosslinking.

The dynamic imbalance of ECM may promote cancer initiation and invasive growth. The developing breast is subjected to several forces that facilitate its normal function (Green and Lund, 2005; Mckenzie et al., 2018). For instance, during the breastfeeding period, the accumulation of milk and alveolar expansion will compress the cavitary epithelial cells of the breast (Stone et al., 2006). Under the action of sucking and oxytocin stimulation, the myoepithelium shrinks and the epithelial cells are subjected to inward tensile stress. In general, the force of healthy breast cavity epithelial cells is in a dynamic equilibrium state throughout the lactation period. In contrast, abnormal tumor anterior cavity breast epithelial cell proliferation is uncontrolled, and the survival rate is enhanced (Ronnov et al., 1996), eventually expands to fill the breast ducts (Kroemer et al., 2015; McDaniel, 2006). In addition, pre-neoplastic lesions secrete a large number of soluble factors, which stimulate immune cell infiltration and activate resident fibroblasts, thereby inducing an osteoproliferation response in the mammary gland and leading to ECM sclerosis (Sickafoose et al., 2006). Over time, the ECM stiffens is a symptom of pre-cancerous (Paszek, 2005; Cassereau et al., 2014). With the development of cancer, the rigid ECM exerts an ever-increasing resistance force on the pre-cancerous duct. Meanwhile, the pre-cancerous luminal epithelial cells invade breast parenchyma to maintain the tension homeostasis of the cellular microenvironment.

As we known, ECM stiffness is not a unique phenotype of breast cancer. In order to research the interaction of ECM structure, composition, and stiffness on the evolution and pathologies of various tumors, researchers have conducted a large number of in vitro experiments, and the experimental results show that cells invasion and migration can be

 Table 1

 Alterations in cell behavior in different pathological conditions and stiffness.

Conditions	Stiffness range	Predominant ECM	Cell phenotypes	Ref.
MMTV PyMT (transgenic mammary tumor)	0.4–4 kPa	Collagen	Stiff ECMs enhanced tumor cell invasion and migration	Levental et al. (2009)
Breast cancer cells	0.2–2.5 kPa	Collagen	Enhanced circulating tumor cells and lung metastasis	Watson (2006)
MDA-MB 231 (breast carcinoma cells)	0.3–2.4 mg/ml	Collagen	Stiff substrates promoted cell invasion	Lang et al. (2015)
Ha-ras (premalignant mammary organoids)	0.2–2.5 kPa	Collagen	Stiff ECMs promoted tumor cell invasion into surrounding ECM	Cassereau et al. (2014)
U373-MG (glioma cells)	0.4–120 kPa	Fibronectin	Stiff ECMs increased cell migration speed	Pathak and Kumar (2012)
MMTV-Neu (Oncogene- initiated mammary tumor)	0.2–2.5 kPa	Collagen	Enhanced tumor cell invasion into surrounding ECM	Rubashkin et al. (2014)

 Table 2

 Performance comparison of common measurement tools.

Туре	Technique	Sensitivity	Limition	Ref.
Single molecule force spectroscopy (SMFS)	AFM	10–10 ⁴ pN	Complicated calculation; Cannot access intracellular structures	Touhami et al. (2004)
	OT	0.1–100 pN	Low throughput Inevitable cellular optical damage	Neuman and Nagy (2008)
	MT	0.01–100 pN	Limited spatial resolution; Irreversible cell damage due to thermal issues	Ayala et al. (2017)
	BFP	10-50 pN	Cannot measure independently	Brody et al., 1995; Chen et al. (2017)
Elastic substrate sensors	TFM	pN	Limited force resolution; Complex equipment and arithmetic; Limited by substrate	Legant et al. (2013); Banda et al. (2019)
	mPDAS	100 nN-50 pN	materials; Limited force resolution; Limited by substrate materials	Polacheck and Chen (2016)

adjusted by changing the stiffness of the substrate (Mammoto et al., 2013;; Gobin and West 2002). On a low rigidity surface, the rate of cell migration speed decreases with matrix stiffness mainly due to increased stability of adhesions (Lang et al., 2015; Pathak and Kumar 2012). For instance, Cassereau and co-workers designed a 3D tension bioreactor system by mechanically adjusting the stiffness of collagen hydrogels, which can accurately assess the effect of ECM hardening on tumor cell invasion (Cassereau et al., 2014; Rubashkin et al., 2014). The research results show that the density and composition of ECM will impose physical restrictions on cell movement and promote cell transformation

(Haage, 2014; Wolf et al., 2013). The stiffness of ECM can directly promote cell invasion and migration.

Cells respond to the mechanical forces or the mechanical properties of their microenvironment that is mostly related to the ECM remodeling and stiffening (Miroshnikova et al., 2011). Normal physiological processes subject cells to various mechanical stimuli (e.g. hydrostatic pressures, shear forces, compressive forces and tensional forces) and cells respond to changes in ECM mechanics by adjusting the structure of the cytoskeleton network. At the same time, changes in cell tension are fed back to the cell ECM, which further regulates the mechanical properties of ECM. Many researchers have previously measured the ECM stiffness or Young's modulus of cells *in vivo* (Table 1). We will summarize and analyze these measurement methods in detail in Section 3 (Table 2).

3. Common measurement tools for cell generated forces

Over the past few years, SMFS methods such as AFM, OT, MT, and bio-membrane force probe (BFP) have been used to measure cell surface single-molecule mechanics. Generally, these methods were applied as the most common procedures for determining the threshold force that result in the dissociation of the ligand-receptor bond on the cell surface. Particularly, TFM mainly rely on electroplating cells onto flexible polymer substrates embedded with fluorescent particles and indirectly measures the receptor force by quantifying the deformation of the substrate. Therefore, the spatial resolution (μ m) and force resolution (μ n) of TFM are limited by polymer crosslink ability. These methods are divided into two categories and are summarized in this section.

3.1. Single molecule force spectroscopy

3.1.1. Atomic force microscopy

AFM was quickly adopted to biology and has been used for decades due to its high resolution coupled with the low-detection limits on the order of pN levels (Touhami et al., 2004; Puech et al., 2006). AFM obtains the relevant force curve by measuring the deflection of the probe (Fig. 2A and B). Describing the cell using a mechanical model, the force curve can be drawn and further analyzed to obtain the Young's modulus, relating its resistance to compressive or tensile forces. Through advanced methods, the cell can be plucked from the substrate, also the adhesion forces of the cell to the surface of the substrate can be measured. Additionally, AFM is also suitable for measuring time-dependent cellular behavior with stress and strain relaxation curves owing to the mature operation and analysis system (Haase and Pelling, 2015; Stylianou et al., 2018). For instance, Cross et al. used AFM to distinguish tumors cells from normal cells, and they found that the flexibility of the cancer cells is different from that of the normal cells (Cross et al., 2007). Jin and co-workers analyzed the influence of aging and Typed 2 diabetes on erythrocytes using AFM. The results of AFM imaging and force-distance measurements show that the adhesion of diseased erythrocytes is significantly enhanced (Fig. 2C) (Hua et al., 2010). Li and co-authors have utilized AFM to map molecular distribution on the surface of cancer cells. They obtained the morphological image of cancer cells, and constructed the distribution map of CD20 on the surface of cancer cells through the analysis of force curves obtained on cell surfaces (Fig. 2D) (Li et al., 2013). This research provides a new method for studying the distribution of cancer cell target protein and drug efficacy. Moreover, AFM provided a reliable technology for analyzing the local mechanical properties of cells through the force distance curve at particular positions with pico-newton sensitivity but cannot achieved a high-resolution topographic imaging.

Recently, topography and recognition imaging (TREC) based on AFM mode with functionalized AFM tips by a ligand has been proposed. For example, Duman et al. used TREC to measure the distribution and the localization of CD1d molecules on THP1 cells loaded with three different glycolipids (a-GalCer, C20:2 and OCH12) (Duman et al., 2013). By

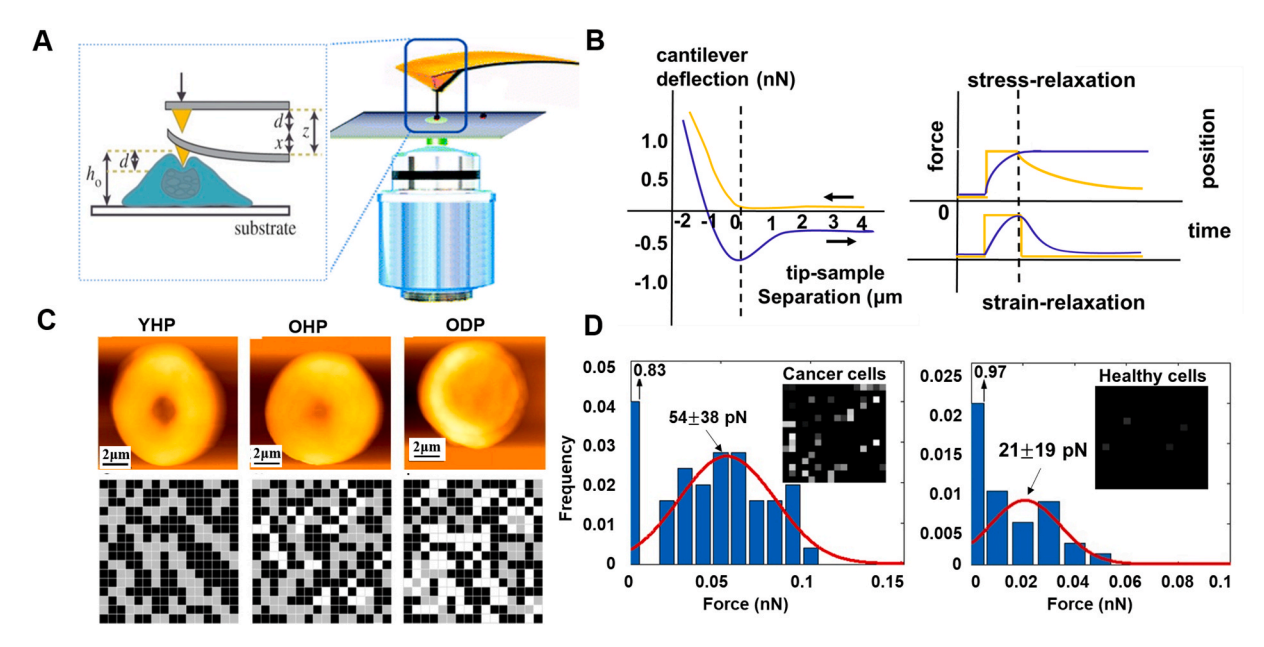


Fig. 2. The basic principle and application of AFM. (A) Schematic of AFM operations. (B) AFM be applied to measure cell elasticity, adhesion, and cell motility over time through simulation of curves and related models. Left: AFM force-indentation curves; right: AFM stress and strain relaxation curves. Reproduced with permission from (Stylianou and Stylianopoulos, 2018). (C) AFM topographic data and AFM force-distance data of YHP (young, healthy people), OHP (old, healthy people), and ODP (old type 2 diabetes patients) erythrocytes. Reproduced with permission from (Hua et al., 2010). (D) The mechanical maps distribution of CD20 and Gaussian fit of the force histograms on the cancer cell and red blood cells (healthy cells). Reproduced with permission from (Li et al., 2013). (For interpretation of the references to colour in this figure legend, the reader is referred to the Web version of this article.)

linking biomolecule onto the AFM tip, Xiao et al. imaged cancer biomarker EGFR in single human breast cancer cells with nanoscale spatial resolution (Xiao et al., 2015). Although TREC combining with AFM has been proven that allows the high spatial (sub-nanometer) and force (pN) resolution with single-molecule force measurement capabilities in physiological environment, it is also limited by cell-substrate contact times of several seconds. To overcome the limit, Sancho et al. proposed a method to measure the intercellular adhesion forces in which the AFM is combined with a microfluidic probe connected to the pump system. With this method, microfluidic probe connected to the pump system provided adsorptive force to immobilize cells without adhesion ligand (Sancho et al., 2017). In addition, recent development in AFM techniques also introduced real-time mapping of the elastic modulus, such as the Peak Force QNM method (Young et al., 2011). These developments reinforce and complement the application of AFM in cell mechanics. However, several issues limit the application of AFM as single cell mechanical sensors in practical biomedical applications (Li et al., 2017a). For example, the throughput is low, the calculation is complicated and time-consuming, and these considerations restrict the further development of AFM.

3.1.2. Optical tweezers and magnetic tweezers

OT and MT are conventional single-molecule manipulation techniques with a similar concept. In both techniques, a micro-particle is manipulated by applying an external force, which can be used for mechanical research of cells and intracellular molecules (Fig. 3A) (Ashkin et al., 1990; Ahmed et al., 2015; Chang et al., 2015; Septiadi et al., 2018). Briefly, a pair of permanent magnets placed above the sample holder of the inverted microscope constitute the central part of the basic MT, and the magnetic field of the magnet generates force. The microscope is equipped with a camera to realize image collection. MT and OT are capable of exerting forces over 1 nN. The ability to stably capture particles from \sim nm to \sim µm scales enables these techniques to be applied to the study of single cells (Fig. 3B) (Neuman and Nagy, 2008). Compared with the traditional biological single-molecule manipulation techniques such as AFM, OT and MT have better manipulation and testing capabilities.

Generally, to study the mechanical properties of cells, optical forces are generated through the interaction between light-manipulatable particles and cells. The light-manipulatable particles can be distributed in cells in three ways: (i) attached to the membrane surface; (ii) embedded in the cytoplasm; (iii) modified to target specific proteins. For instance, to research the influence of medicine on the mechanical properties of cells, Ayala's team put the light-manipulatable particle on the cell membrane, and by pulling the particles, the cell membrane was deformed to produce an extension similar to a tether (Ayala et al., 2017). They derived the mechanical parameters of the cell membrane through the tether parameters. The results of the experiment showed that three different drugs, Blebbistatin (BBI), Cytochalasin D (CytoD), and Jasplakinolide (JPK), all caused changes in the cytoskeleton structure of actin, and reduced cell membrane tension due to the decreased stability of the cytoskeleton (Fig. 3C) (Ahmed et al., 2015). Furthermore, Nawaz and co-workers investigated the mechanical response of the F-actin cytoskeleton using OT with particles embedded in the cytoplasm (Nawaz et al., 2012). Additionally, studying of the aging of erythrocytes during storage in an ex vivo environment, they used optical trapping experiments without particles. In the 21 days of the experiment, the light beam directly stretched the cells. In the end, it was estimated that the red blood cell membrane shear modulus increased from 2.5 to 13 $\mu N/m$ (Czerwinska et al., 2015).

Due to the sensitivities of many cells to high-power lasers, the damage induced by OT limits its further applications in biology. With the development of nanomaterials, luminescence-concentrating upconversion nanoparticles (UCNPs) have been integrated with OT provides a significant signal amplification approach to instead high-power lasers, and thus the damage to cells caused by high-laser was effectively reduced (Li et al., 2020). Meanwhile, a new technology known as near-field OT has provided more convenience to trapping particles than its far-field counterparts with limited Rayleigh length (Hu et al., 2020). Additionally, the high throughput of MT has been utilized to study the mechanical forces of cellular actin and the cytoskeleton (Wang et al., 1993; Matthews et al., 2006; Tseng et al., 2012). However, the popularity of MT is mainly attributed to its ability to manipulate, and importantly rotate, magnetic particles. This feature allows MT to

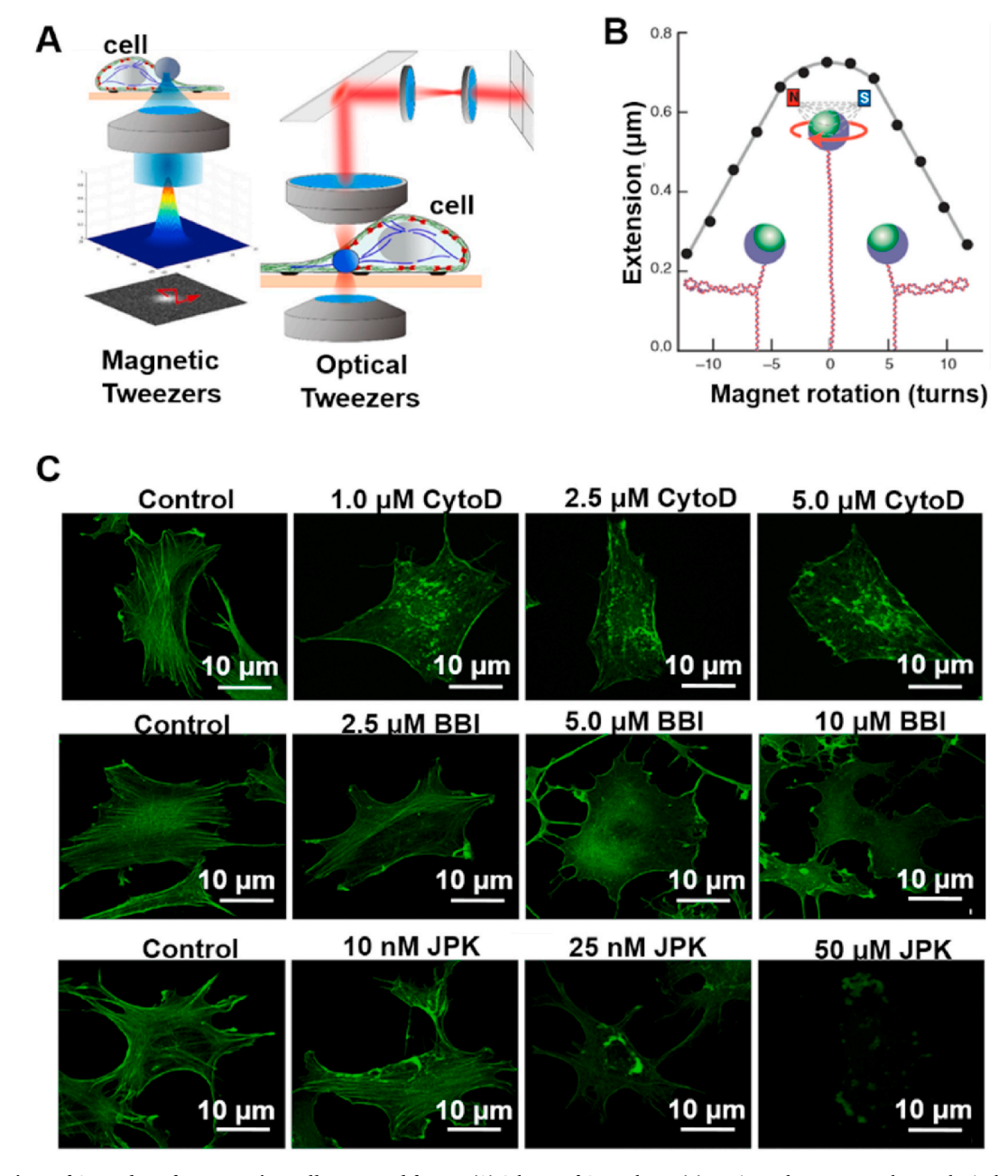


Fig. 3. Applications of OT and MT for measuring cell generated forces. (A) Scheme of OT and MT. (B) MT is used to measure the topological structure of DNA. The curve shows the extended rotation function of the 1 μ m superparamagnetic beads that bind 3 kb DNA molecules on the surface under a tension of 0.4 pN. Reproduced with permission from (Neuman and Nagy, 2008) (C) Representative images of NIH3T3 cells stained for Phalloidin-FITC related to various drugs with different concentrations. Reproduced with permission from (Ayala et al., 2017).

directly study the effects of torque and twist on the dynamics of biomolecular interactions, so it is commonly used to study the folding dynamics of nucleases and DNA (Herrerogalan et al., 2013; Ding et al., 2012; Chen et al., 2015, Dong et al., 2020).

3.1.3. Bio-membrane force probe

The BFP is one of the most common sensitive force technique for determining molecular adhesion and structural linkages at biological interfaces (Evans et al. 1995). BFP is based on the microtubule suction method, which can capture cells or microspheres that characterize specific interacting molecules, and can achieve the process of approach-contact-retraction of cell-cell by manipulating microtubules (Fig. 4A) (Brody et al., 1995). During this dynamic process, the deformation of the cell and the obtained force distance curves are used to study the mechanical properties of the cell membrane. BFP was applied

to characterize the single-molecule dynamics of living cells due to the low spring constant, high biocompatibility, and user-friendly maneuverability (Ju and Zhu, 2017). The proposal of BFP is helpful for the study of cell adhesion mechanics and the study of the bonding force of single molecules on the cell membrane. Courier's team used BFP to study the binding process of oocytes and sperm, measured the local changes in gamete membrane adhesion, and probed the mechanical properties of the oocyte membrane on the micrometer scale (Gourier et al., 2008). Zhu and co-workers demonstrated the ability of BFP to characterize the structural mechanics of proteins on the cell membrane. The experimental results show that when the adhesion force exists, it remains stable around the preset value until it dissociates, which reflects the sustainability of the bond under a given force (Fig. 4B) (Chen et al., 2017). And they proved the BFP assay test specificity, not express (black), wild-type (magenta), express integrin $\alpha V\beta 3$ (D723R, green) or

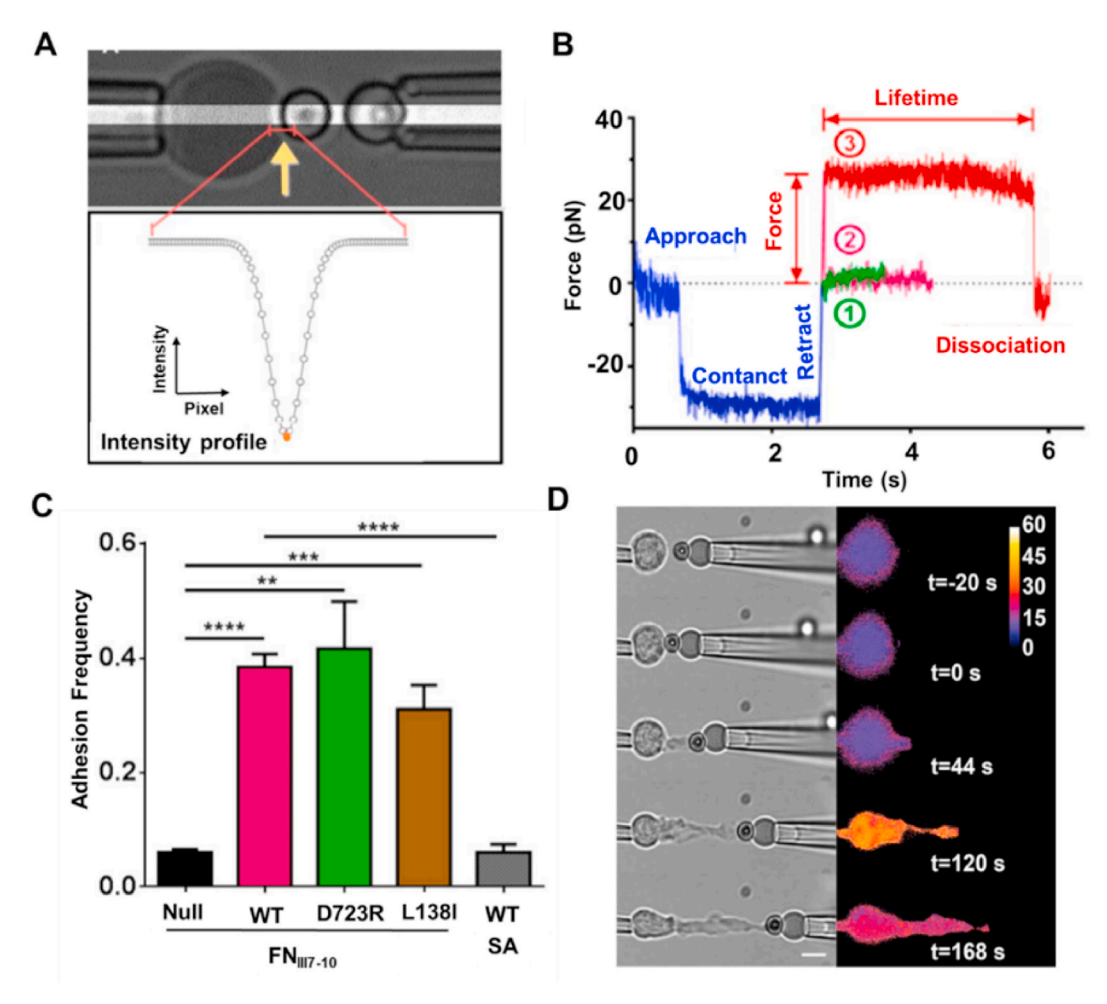


Fig. 4. Application of BFP for measurement of cell adhesions. (A) Scheme of BFP: probe of the BFP composed by a biotinylated erythrocyte and a strep avidinated glass bead. Reproduced with permission from (Brody et al., 1995). The subgraph represents the strength of the interaction force between two cells or molecules that can be captured. (B) The duration of the force-clamp phase was measured as the bond lifetime. The initial condition of the experiment is to drive the target cell close to the probe beads, contact for 2 s under a pressure of about 30 pN, and then retract (blue). The force would return to zero, if there were no adhesion (1, green). If there is strong adhesion, the adhesion force rises from zero (2, purple) to the preset force (3, red, 25 pN as shown), and then remains constant until it returns to zero after dissociation. During of the time is regarded as the bond lifetime. (C) Binding specificity tests. Adhesion frequencies between cells expressing control, WT, D723R, or L138I integrin $\alpha V\beta 3$, and between the SA bearing probe and cells expressing WT integrin. Reproduced with permission from (Chen et al., 2017). (D) Successive phases during the interaction of a T cell with an anti-CD3 coated bead on the BFP. Reproduced with permission from (Julien et al., 2011). (For interpretation of the references to colour in this figure legend, the reader is referred to the Web version of this article.)

(L138I, brown), and between the streptavidin (SA) bearing probe and cells expressing wild-type (WT) integrin (gray) (Fig. 4C). In order to explore the mechanical properties of T cell receptors and function-associated antigen 1 (LFA-1) during T cell activation, Julien and collaborators used BFP and APC models to conduct experiments. The experimental results show that T cells are accompanied by mechanical response mechanisms early in the activation process, and the loading rate during the pulling phase increased with the target stiffness (Fig. 4D) (Julien et al., 2011). Despite its successes, there are drawbacks. For instance, BFP often requires additional techniques to assist in depth analysis and obtain conclusions. Moreover, there is no suitable cell microsphere model. Therefore, the Young's modulus cannot be deduced from the force-distance curve. Fortunately, recent advances in fluorescence imaging technology and dual devices have promoted BFP as a useful tool for visualizing cellular mechanical events (Ju and Zhu, 2017; Ju et al., 2017; Liu et al., 2014).

3.2. Elastic substrate sensors

The second category of common cellular force measurement is the sensors based on elastic substrates, which play a dominant role in

measuring the mean traction force at a cellular or subcellular scale (Guo et al., 2014). SMFS methods use beads or cantilevers to attach to cells, in contrast to these methods, substrate based methods use cells cultured on elastic polymers or microstructures that deform under cell-generated forces. Generally, the mechanical force measured by this method is reflected by the deformation of the elastic structure or the movement of the fluorescent particles in the substrate (Polacheck and Chen, 2016). Here, we will review the two most common methods TFM (Fig. 5A) and mPADs (Bergert et al., 2016).

3.2.1. Traction force microscopy

The physical and mechanical interaction between the cell and the ECM microenvironment involves many complex biological signal transduction pathways. It plays an essential role in regulating cell proliferation, differentiation, and migration. In 1980, Harris and coworkers were the first to use cell traction force microscopy. The initial experiments used cultured fibroblasts on a silicone film, and for the first time, the deformation of the film was observed and measured to estimate the cell traction force (Harris et al., 1980). Subsequently, TFM has developed into a method to measure cell-generated forces at the single cell level thanks to the ability to visualize cell structures easily in TFM.

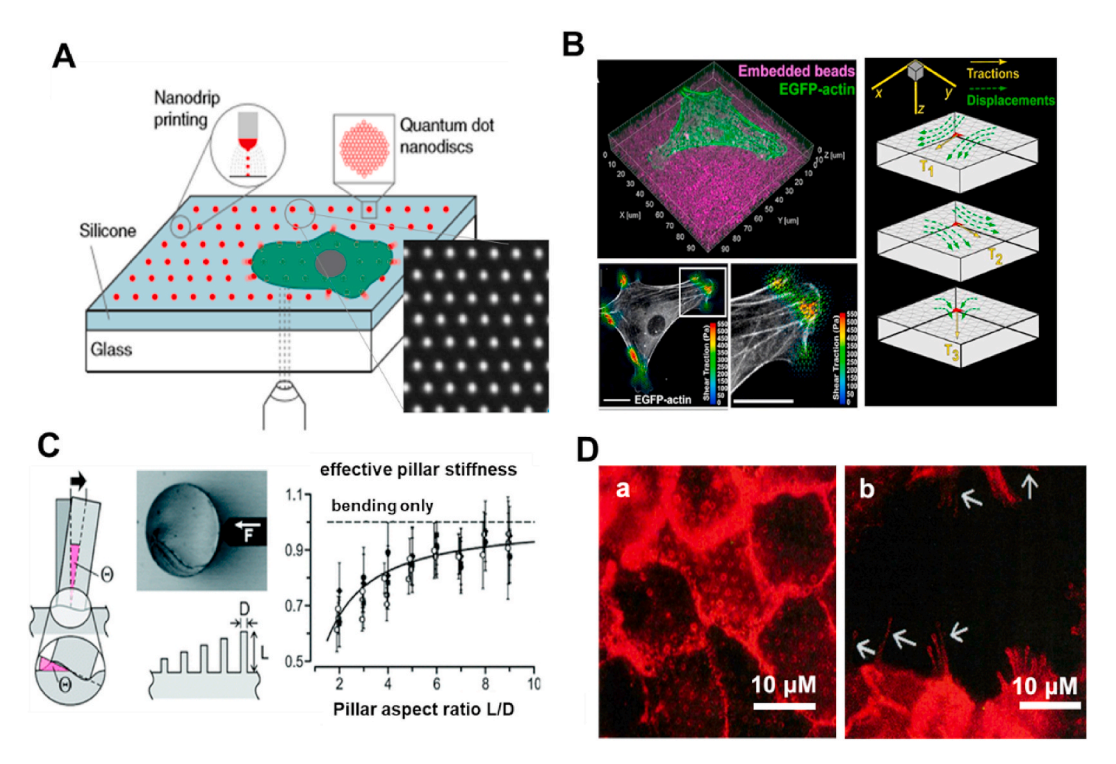


Fig. 5. Methods for measuring forces exerted by cells on surrounding substrates. (A) Overview and characterization of the TFM platform. (B) Characterization of out-of-plane rotational moments about FAs using a high-resolution 2.5D TFM. Upper left: Mouse embryonic fibroblasts (MEF) completely diffuse and polarized on the plane; bottom left: shear and normal traction stress vectors on the cell body and the zoomed image of the boxed region; right: the finite element model used in the experiment. Reproduced with permission from (Sabass et al., 2008). (C) Illustration of the mPADs. The micropillars of mPADs are subjected to horizontal force F, which causes the micropillars to deform. Evaluate cellular mechanical force by establishing the relationship between the deformation of the pillar and the force, which influenced by pillar stiffness and pillar diameter (D) and height (L). Reproduced with permission from (Schoen et al., 2010). (D) mPADs to quantify the directional migration of actin. Images of the distribution of actin in the normal monolayer(a) and the distribution after 6 h (b). The white arrow in b indicates the actin-rich fibril structure due to the dissociation of the epithelium. Reproduced with permission from (Du Roure et al., 2005).

Especially, the focal adhesions (FAs) formed by cells and elastic substrates, it is easy to determine the size of FAs and calculate the traction force exerted by these structures through the deformation of the flexible substrate (Banda et al., 2019; Goktas and Blank, 2017). Plotnikov and co-workers utilized high-resolution time-lapse TFM to characterize the traction force distribution and dynamics of a single mature FA in fibroblasts (Sabass et al., 2008). Studies have shown that FAs exhibit stable and dynamic traction regulated by specific signaling pathways. The dynamic fluctuation of traction in FAs is closely related to guiding cell migration. Conventional TFM reflects the cell force in the 2D plane, but to measure 3D forces exerted by cells on 2D planar surfaces, Legant and co-workers developed a high-resolution 2.5D TFM (Fig. 5B). The study revealed a 3D traction force distribution during cell migration and explained that these traction forces would generate rotational torque and propagate along the front of the cell (Legant et al., 2013). Furthermore, a newly developed 3D TFM has been shown to accurately determine cell traction forces in three dimensions during cell migration (Franck et al., 2011). The basic principles of TFM lead to some limitations. For instance, the elastic deformation of the substrate is determined by tracking the randomly distributed fluorescent particles' displacement in the substrate. Randomly distributed fluorescent particles lack the control of the position and spacing of the fiducial marks, which may cause problems such as subsequent stress calculation errors. Methods have been proposed to overcome these limitations (Banda et al., 2019; Legant et al., 2013; Desai et al., 2007). The force resolution of TFM is on the order of pN, but the complexity of its later inversion algorithms hindered further research in the biological field. It is inevitable that more in-depth studies by TFM at the cellular level depend on the emergence of more sophisticated equipment and algorithms.

3.2.2. Micropost array detectors

Micropost array detectors (mPADs) are an additional way to reversely attain a force value from the deformation of the elastic substrate. Compared with TFM, the substrate is composed of micropillars with a size of 0.5–10 μm. The micropillars are arranged in an array with known position and spacing, which overcomes the defects of classical TFM. Furthermore, understanding the elastic deformation of the microcolumn and spring constant k, the magnitude of the forces can be calculated using Hooke's law (Fig. 5C), which significantly reduces the calculation cost relative to TFM. Based on these advantages, mPADs can be applied to the measurement of multi-cell populations (Schoen et al., 2010; Trepat et al., 2009). At the single cell level, mPADs found widespread applications to study cell-cell interaction, cell migration, and the interactions between force and FAs (Liu et al., 2010; Maruthamuthu et al., 2011; Rabodzey et al., 2008). For instance, Rathod et al. showed migration trajectories of fibroblasts along the substrate ridges and calculated the contour plot of the traction forces (Rathod et al., 2017). Roure and his team used a multi-particle tracking method and a high-density elastic micropillar array to measure the dynamic traction force of MDCK epithelial cells. Regarding the mechanical force distribution of MDKC cells, the experimental results showed that the maximum force on the surface was concentrated on the edge and protrusion area of the cell. The average traction force at the cell edge was about 5 nN with a maximum of 20 nN (Fig. 5D) (Du Roure et al., 2005). Therefore, it has many advantages in studying cell migration and cell adhesion mechanics, such as mPADs are easy to implement, simple to calculate, and can detect a force in the range of 50 pN~100 nN (Polacheck and Chen, 2016). However, single cell level and even subcellular studies often require higher force resolution. For example, the force transmitted by the receptor ligand bond on the cell surface is much less than 50 pN, so there is still no advantage for cell mechanical research at

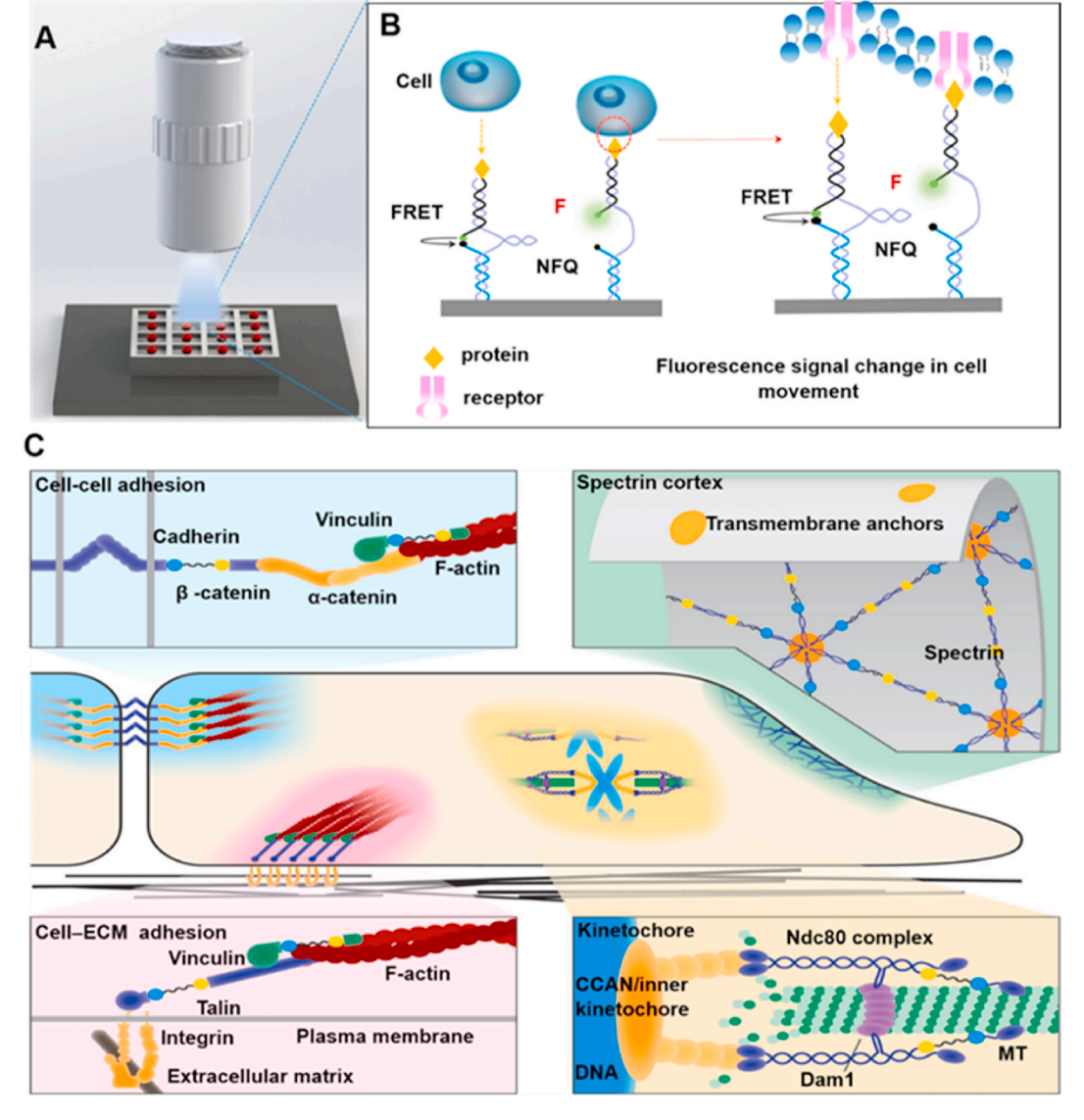


Fig. 6. Single cell mechanics measurement platform. (A) Schematic of the single cell array. The submap in (B) showing the expected mechanism of how cell-generated forces activate the DNA tension sensor. (C) The figure illustrates the mechanical devices of cell-cell connection, cell-matrix adhesion, and molecular transfer between cells. The sub-picture shows that FRET-based tension sensors were modified by adhesion (E-cadherin, VE-cadherin, and vinculin) to detect molecular mechanics in cell-cell junctions (blue part) and propagation of mechanical force during cell-matrix adhesion (red part). To evaluate the mechanical force of the cell cortex (green part), FRET-based tension sensors have been combined with spectrin (a stretchable fibrous protein). And the tension sensors are applied to real-time monitoring of the mechanical changes during cell mitosis. Reproduced with permission from (Guo et al., 2014). (For interpretation of the references to colour in this figure legend, the reader is referred to the Web version of this article.)

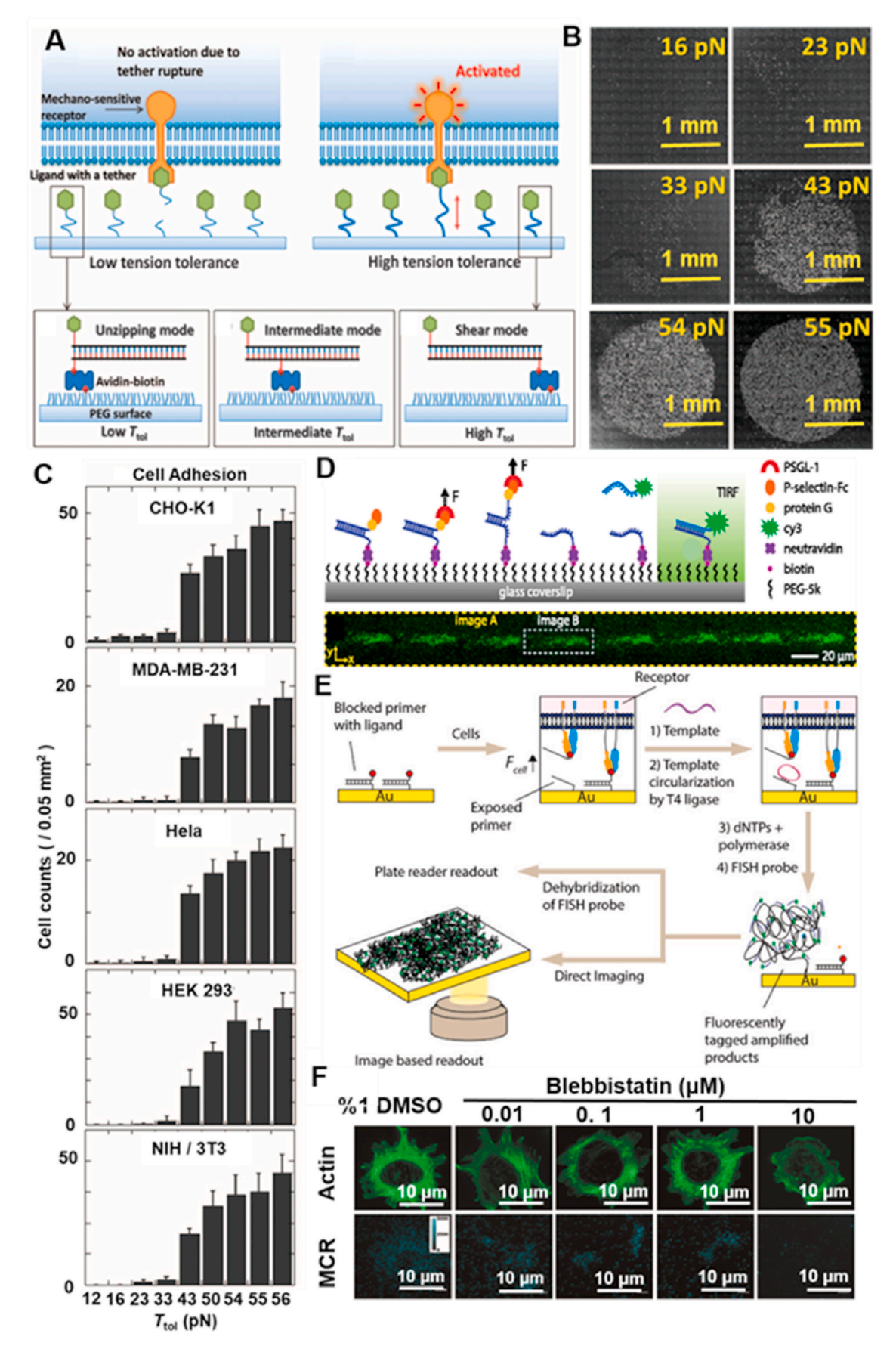
a deeper level with mPAD.

4. Micro and nanoscale mechanical sensors

Recently, FRET-based tension sensors have been widely used in the study of dynamics in living cells, as well as single cell arrays are designed to study the mechanical conduction between molecules (Fig. 6A) (Stabley et al., 2012; Liu et al., 2013). The FRET-based tension sensor consists of a biomolecular spring labeled with a donor-acceptor pair on both sides (Wang et al., 2016; Golser et al., 2017). The elongation of the natural spring can lead to an increase in the distance between the two fluorescent proteins and a decrease in FRET efficiency (Dong et al., 2020a,b). It is possible to infer the mechanical changes in the cell by detecting the change in FRET efficiency (Fig. 6B). The change in FRET efficiency between the fluorescent donor and the acceptor can convert the mechanical transmission of the skeleton structure into an optical signal. In particular, the spring-like linker must have spring flexibility

that meets the universal biological tension range (\leq 100 pN) (Chowdhury et al., 2016; Zohar et al., 2010). Theoretically, it has the highest tension sensitivity when there is no external load.

Currently, FRET-based tension sensors were used to quantitatively detect mechanical properties of the molecular process of cell surface proteins (Fig. 6C, red part) (Chen et al., 2017) and the mechanical force changes during cell mitosis were (Fig. 6C, yellow part) (Li et al., 2019; Yan et al., 2017). Also, the mechanical transmission between cells was measured using the binding of vinculin and catenin (Fig. 6C, blue part) (Aird et al., 2020) and the tension of the cell cortex was analyzed by the scalability of spectrin (Fig. 6C, green part) (Gourer et al., 2008). Moreover, FRET-based tension sensors have been demonstrated to be one of the most well-known tools for assessing unravel force transduction mechanisms. This section highlights the development of FRET-based DNA tension sensor for live-cell force sensing-a nascent but rapidly growing area of research. Mechanical DNA devices have been enabled by the accessibility, versatility, and precision of DNA-based



(caption on next page)

Fig. 7. DNA-based tension gauge tether and its variants. (A) Tension gauge tether is dissociable dsDNA modified ligands. A designated rupture force (T_{tol}) of the dsDNA-based TGT can be evaluated depending on the anchor position of the ligand. (B) Confocal fluorescent images of CHO–K1 cells. The mechanical distribution of the cell surface is measured at the TGT breaking force (T_{tol}) at 16–55 pN. Reproduced with permission from (Wang and Ha, 2013). (C) Cell adhesion on TGT with RGD. (D) Schematic of FISH based TGT. The cell migration force is higher than T_{tol} , leading to hydrogen bond breakage, the exposed ssDNA is combined with the free Cy3 labeled complementary strand, and the fluorescent signal turns on. Reproduced with permission from (Li et et al., 2017). (E) Process of TGT-based MCR. when the tether breaks, it uses enzymes to effectively convert the exposed primers generated by TGT fragmentation into fluorescent signals that can be detected by a fluorescence microscope. Reproduced with permission from (Ma et al., 2016). (F) Representative fluorescence images showing F-actin staining and MCR signal for NIH/3T3 cells treated with increasing concentrations of BBI. Reproduced with permission from (Ma et al., 2016).

design. In this section, the FRET-based DNA tension sensor is divided into TGT and DNA hairpin force probes according to the structure.

4.1. Tension gauge tethers

The TGT is a ligand labeled DNA oligonucleotide that was initially developed to measure the magnitude of peak tension experienced by the receptor (Yamashita et al., 2016; Wang and Wang, 2016). The tension of the TGT can establish a dynamic measurement range by changing the anchor position, and the peak force of TGT changes with the movement of the anchor position. When cells are cultured on a substrate covered by TGT, the cell tension forces exceeded the peak forces of TGT, the tether is broken, and mechanical signal transmission is eliminated (Fig. 7A and B) (Wang and Ha, 2013). On the contrary, cell tension forces lower than the peak force have resulted in the quenching between both fluorophores. For example, Wang et al. designed a programmable tension-regulating TGT, using ssDNA as a tension tether. The peak tension of the TGT ranged from 12 to 56 pN and were tested with several cell lines. Experimental results confirmed that the mechanical force for cell diffusion is more excellent than 40 pN (Fig. 7C). In 2017, the Li lab directly used surface-immobilized ssDNA as the docking sequence of fluorescence in situ hybridization (FISH) to detect the mechanical characteristics distribution of leukocyte surfaces. The experimental results showed a periodic patchy yet highly asymmetric adhesion footprint on the cell surface (Fig. 7D) (Li et al., 2017a,b,c).

Besides, the TGT has been improved by combining the affinity between the DNA binding protein and DNA. Ha and co-workers determined that separate a poly-T₆₅ DNA sequence from this ssDNA binding protein only requires 4 pN of force and they exploited this phenomenon to design a new generation of TGT with lower force. The detection range has been expanded from 4 pN to 56 pN. However, the TGT irreversibly ruptures at a sequence specific tension threshold between 4 pN to 56 pN, limiting the maximum force applied by cell receptors and DNA binding protein. Subsequently, Garcia's research group combined with polymerase chain reaction (PCR) analysis methods to improve the TGT probe, effectively converts mechanical force into amplified fluorescence readings, which was called mechanically induced catalytic amplification reaction (MCR) (Luca et al., 2017). The working principle of MCR is to use TGT as a peak force sensor, once the tether breaks, the dissociated ssDNA as a primer for rolling circle amplification, to produce ssDNA with long tandem repeats (Fig. 7E) (Ma et al., 2016). Subsequently, the experimental results prove the MCR signal displayed a dose-dependent relationship, where the highest BBI concentrations generated the lowest MCR signal (Fig. 7F). The signal intensity of MCR depends on the number of broken probes and amplification conditions, which is related to the incubation time.

4.2. DNA hairpin force probe

Compared to the irreversible TGT that cannot refold upon rupturing, the DNA hairpin force probe is reversible and digital. DNA hairpin force probes consist of a re-foldable DNA hairpin stem-loop and employs DNA hairpins as a switch element (Han and Rooij, 2016; Ma and Salaita, 2019; Brasko et al., 2018). The required force ($F_{1/2}$) to unfold the stem-loop structure can be controlled by the length of the DNA hairpin and the nucleotide guanine (G) and cytosine (C) base pairs content. Firstly, the donor and an acceptor are placed nearby and are in a

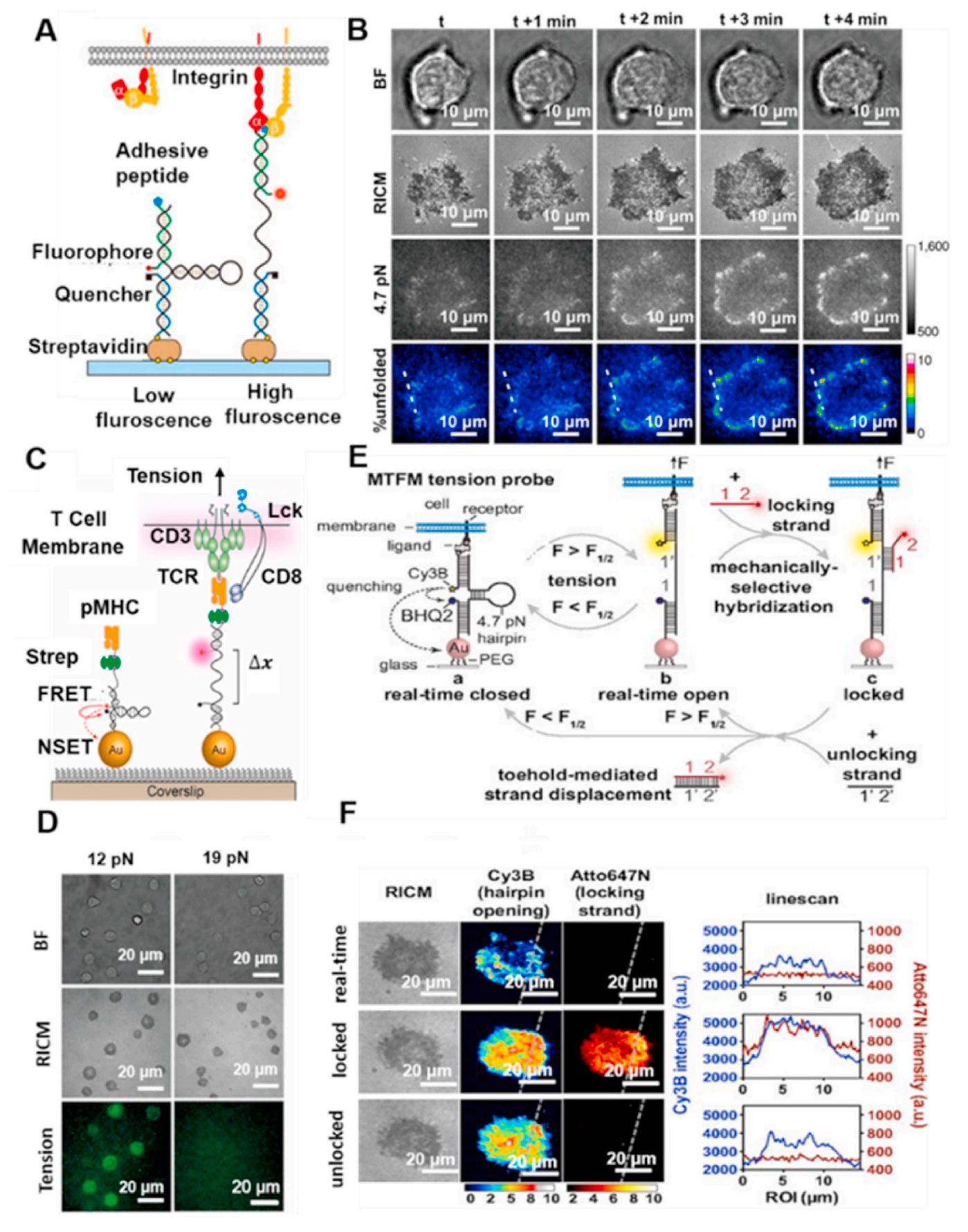
quenched state. When the DNA hairpin is pulled by force greater than $F_{1/2}$, the stem-loop structure will unfold, separating the donor from the acceptor and causing the fluorescence emission to recover.

The DNA hairpin force probe is often used to detect cell surface receptor forces and transient mechanical responses because of it have highly cooperative and a well-defined force response. The first generation of hairpin force probes was reported in 2014, which were developed to reveal integrin forces during early cell adhesion (Fig. 8A) (Zhang et al., 2014). The probe is decorated with a donor and acceptor and a biological ligand and is immobilized on a glass surface by biotin-streptavidin interaction. The study showed the dynamic tension distribution during cell diffusion and adhesion and found that a subset of integrin was pulled with force in the range of 4.7 pN to 13.1 pN (Fig. 8B). Subsequently, due to the problem of biotin-streptavidin dissociation in the first generation of hairpin force probes, the DNA-based AuNP force probe was reported in 2016, which enhanced sensitivity and stability (Liu et al., 2016) Compared to the first DNA hairpin force probe, this probe was functionalized with a terminal thiol group enabling the formation of a gold-thiol bond (Fig. 8C). This method can produce double quenching, which causes a 100-fold fluorescence enhancement, which is 20 times that of the first DNA hairpin force probe. This probe was used to research force transmission in TCRs, and results showed that T cells are coupled through the cytoskeleton and transmit a 12 pN-19 pN force to TCRs during binding to the ligand (Fig. 8D).

Traditional probes rapidly refold upon termination of the mechanical input, resulting in quenching of fluorescence. Thus, the probes fail to capture rare mechanical events or transient mechanical events with a lifetime below that of the fluorescence acquisition time window (>100 ms) (Juette et al., 2014; Yin and Zhao, 2011). Recently, Salaita's group reported a DNA hairpin force probe with the concept of dynamic mechanical information storage (Fig. 8E) (Ma et al., 2019). They introduced the locking strand and unlocking strand to achieve the function of recording and erasing molecular force signals. Considering a transient mechanical event in the cell, it may be possible that the probe is unfolded and refolded over a short period of time before observation, resulting in this part of the force being missed. After the lock chain is added, the probe can remain pulled apart after unfolding, and therefore mechanical information can be stored. The experiment also introduced the unlocking strand, which is a piece of base sequence that can detach the locked strand that has been bound to the DNA probe so that they can bind to each other. The experiment confirmed that the probe could enhance the fluorescence intensity; that is, it stores a part of instantaneous mechanical information. For example, T cells were allowed to adhere and spread on MTFM probe surfaces presenting anti-CD3e antibodies. Cells generated tension signal as the TCR engaged the antibody and transmitted forces to the probes (Fig. 8F). However, DNA mechanical probes can be damaged by time and the external environment. For example, the serum in the culture medium that maintains the normal life activities of cells is rich in nucleases, and some cells themselves secrete proteases and nucleases. These enzymes will cause irreversible chemical damage to the DNA probe, thus causing difficulties in mechanical measurement.

5. Outlook

The importance of mechanotransduction at single cell resolution has been widely recognized, as each cell displays distinct characteristics, for



(caption on next page)

Fig. 8. DNA hairpin force probes and its variants. (A) Schematic of the integrin tension sensor. (B) Representative time-lapse images showed the change in force signal during the initial stages of cell spreading and adhesion. Reproduced with permission from (Zhang et al., 2014) (C) Schematic of DNA-based AuNP force probe for mapping TCR-mediated tension; (D) Representative brightfield, RICM, and tension images of OT-1 cells cultured on tension probe surface modified with N4 pMHC. These cells were able to open probes with $F_{1/2} = 12$ pN, but unable to open probes with $F_{1/2} = 19$ pN. Reproduced with permission from (Liu et al., 2016). (E) Schematic of DNA hairpin force probe with the concept of dynamic mechanical information storage. (F) RICM, Cy3B, and Atto647N TIRF images of locking/unlocking process with single OT-1 cell. The dashed line in the fluorescence images corresponds to the raw intensity lines can profile shown to the right. Reproduced with permission from (Ma et al., 2019).

which the investigation of cellular clusters might lose key information concerning the heterogeneity and the origin of the cellular mechanical interaction. For measuring the cellular forces, SMFS methods, including AFM, OT, MT and BFP, have shown limitations on their low-throughput, complicated calculation, time consuming processing, and stiffness data susceptible to incorrect fitting. In contrast to SMFS, one issue associated with TFM and mPADs lies in the fact that the spatial resolution (µm) and force resolution (nN) are limited by the crosslinking properties of polymers. The recent advances in FRET sensors show promise to analyze pN-level tensions within cells, under targeted binding with receptors on the cell membrane. The FRET sensors not only achieve sub-cellular resolution, but also provide visualization of the force distribution over the cell. However, current experiments use information from hundreds of molecules to determine an average FRET efficiency, and thus an average force per molecule. This is a problem of the system because not all binding proteins will bind to FRET probes to generate mechanical signals. In addition, with the rapid development in DNA nanotechnology, DNA-based tension sensors convert mechanical events into fluorescent signals by the synthesis of the fluorophores-mechanical receptor complex. Both methods enable quantifying the amplitude and the direction of forces of live cells. However, the limitations include nuclease degradation, short working time, and complications in sensor modification, among others. At present, an exciting frontier would be to improve the current DNA based tension technology such that automation and real-time tracking of cell traction forces may be achieved, thereby providing new insight into cell behaviors. It is well known that there is heterogeneity in ECM (constituents, architectures, and mechanical) in different areas of the same tumor. Therefore, the measurement of local mechanics of the diseased tissue combined with local pathological analysis provides an effective approach to explore how the ECM mechanics influence tumor progression and fate.

Declaration of competing interest

The authors declare that they have no known competing financial interests or personal relationships that could have appeared to influence the work reported in this paper.

Acknowledgments

LC acknowledge the funding support from the NSFC (No. 32071407 and No. 62003032). RY acknowledge the funding support from the NSF (award #1826135, #1936065), the NIH P20GM113126 (Nebraska Center for Integrated Biomolecular Communication) and P30GM127200 (Nebraska Center for Nanomedicine), the Nebraska Collaborative Initiative and Nebraska EPSCoR FIRST award.

References

```
Ahmed, W., Fodor, E., Betz, T., 2015. Biochim. Biophys. Acta Mol. Cell Res. 1853 (11),
    3083-3094.
```

```
Bergert, M., Lendenmann, T., Zündel, M., Ehret, A.E., Panozzo, D., Richner, P., Kim, D.K.,
     Kress, S.J.P., Norris, D.J., Sorkine-Hornung, O., 2016. Nat. Commun. 7, 12814.
Brasko, C., Smith, K., Molnar, C., Farago, N., Hegedus, L., Balind, A., Balassa, T.,
     Szkalisity, A., Sukosd, F., Kocsis, K., 2018. Nat. Commun. 9 (1), 226.
Brody, J.P., Han, Y., Austin, R.H., Bitensky, M., 1995. Biophys. J. 68 (6), 2224–2232.
Butcher, D.T., Alliston, T., Weaver, V.M., 2009. Nat. Rev. Canc. 9 (2), 108–122. Carlton, J.G., Jones, H., Eggert, U.S., 2020. Nat. Rev. Mol. Cell Biol. 21 (3).
Carvalho, F.A., Connell, S.D., Miltenbergermiltenyi, G., Pereira, S.V., Tavares, A.,
     Ariens, R.A.S., Santos, N.C., 2010. ACS Nano 4 (8), 4609-4620.
Cassereau, L., Miroshnikova, Y.A., Ou, G., Lakins, J., Weaver, V.M., 2014. J. Biotechnol.
    193, 66-69.
```

Chang, L.Q., Howdyshell, M., Liao, W., Chiang, C., Gallego-Perez, D., Yang, Z., Byrd, J., Wu, L., Muthusamy, N., Lee, L.J., Sooryakumar, R., 2015. Small 11, 1818-1828. Chen, H., Yuan, G., Winardhi, R.S., Yao, M., Popa, I., Fernandez, J.M., Yan, J., 2015. J. Am. Chem. Soc. 137 (10), 3540-3546.

Chen, Y., Lee, H., Tong, H., Schwartz, M.A., Zhu, C., 2017. Matrix Biol. 60 (16), 70-85. Chowdhury, F., Li, I.T.S., Ngo, T.T.M., Leslie, B.J., Kim, B.C., Sokoloski, J.E., Weiland, E., Wang, X., Chemla, Y.R., Lohman, T.M., 2016. Nano Lett. acs.nanolett 6b01403.

Cost, A.L., Ringer, P., Chrostek-Grashoff, A., Grashoff, C., 2015. Cell. Mol. Bioeng. 8 (1),

Cross, S.E., Jin, Y., Rao, J., Gimzewski, J.K., 2007. Nat. Nanotechnol. 2 (12), 780-783. Czerwinska, J., Wolf, S., Mohammadi, H., Jeney, S., 2015. Cell. Mol. Bioeng. 8 (2), 258-266.

Desai, R.A., Yang, M.T., Sniadecki, N.J., Legant, W.R., Chen, C.S., 2007. J. Visualized Exp. (8) 311-311.

Ding, F., Manosas, M., Spiering, M.M., Benkovic, S.J., Bensimon, D., Allemand, J., Croquette, V., 2012. Nat. Methods 9 (4), 367-372.

Dong, Z.Z., Jiao, Y.L., Xie, B.T., Hao, Y.C., Wang, P., Liu, Y.Y., Shi, J.F., Chitrakar, C., Black, S., Wang, Y.C., Lee, L.J., Li, M., Fan, Y.B., Chang, L.Q., 2020a. Microsyst. Nanoeng. 6 (1), 2-11.

Dong, Z.Z., Xue, X.Y., Liang, H.L., Guan, J.J., Chang, L.Q., 2020b. Anal. Chem. https:// doi.org/10.1021/acs.analchem.0c03518.

Du Roure, O., Saez, A., Buguin, A., Austin, R.H., Chavrier, P., Silberzan, P., Ladoux, B., 2005. Proc. Natl. Acad. Sci. Unit. States Am. 102 (7), 2390-2395.

Duman, M., Chtcheglova, L.A., Zhu, R., Boznaa, B.L., Polzellad, P., Cerundolod, V., Hinterdorfer, P., 2013. J. Mol. Recogn. 26 (9), 408-414.

Dupres, V., Alsteens, D., Wilk, S., Hansen, B., Heinisch, J.J., Dufrene, Y.F., 2009. Nat. Chem. Biol. 5 (11), 857-862.

Eder, D., Basler, K., Aegerter, C.M., 2017. Sci. Rep. 7 (1).

Evans, E., Ritchie, K., Merkel, R., 1995. Biophys. J. 68 (8), 2580-2587.

Franck, C., Maskarinec, S.A., Tirrell, D.A., Ravichandran, G., 2011. PloS One 6 (3).

Freikamp, A., Cost, A., Grashoff, C., 2016. Trends Cell Biol. 26 (11), 838-847. Geiger, B., Spatz, J.P., Bershadsky, A.D., 2009. J. Nat. Rev. Mol. Cell Biol. 10 (1), 21-33.

Gobin, A.S., West, J.L., 2002. West. Faseb. J. 16 (7), 751. Goktas, M., Blank, K., 2017. Adv. Mater. Interfaces 4 (1), 1600441.

Golser, A., Roeber, M., Boerner, H., Scheibel, T., 2017. ACS Biomater. Sci. Eng. acsbiomaterials 7b00583.

Gourier, C., Jegou, A., Husson, J., Pincet, F., 2008. Cell. Mol. Bioeng. 1 (4), 263-275. Green, K.A., Lund, L.R., 2015. Bioessays 27 (9), 894-903.

Guedes, A.F., Carvalho, F.A., Malho, I., Lousada, N., Sargento, L., Santos, N.C., 2016. Nat. Nanotechnol. 11 (8), 687-692.

Guo, J., Sachs, F., Meng, F., 2014. Antioxidants Redox Signal. 20 (6), 986-999.

Haage, A., Schneide, I.C., 2014. Faseb. J. 28 (8), 3589-3599.

Haase, K., Pelling, A.E., 2015. J. R. Soc. Interface 12 (104), 20140970-20140970.

Han, M.K.L., De Rooij, J., 2016. Trends Cell Biol. 26 (8), 612-623. Harris, A.K., Wild, P., Stopak, D., 1980. Science 208 (4440), 177-179.

Herrerogalan, E., Fuentesperez, M.E., Carrasco, C., Valpuesta, J.M., Carrascosa, J.L., Morenoherrero, F., Ariasgonzalez, J.R., 2013. J. Am. Chem. Soc. 135 (1), 122-131. Holmbeck, K., Szabova, L., 2010. Birth Defects Res., Part C. 78 (1), 11-23.

Hu, S., Liao, Z.W., Cai, L., Jiang, X.X., 2020. Phys. Status Solidi (1), 217, 2020.

Hua, J., Xing, X., Zhao, H., Yong, C., Cai, J., 2010. Biochem. Biophys. Res. Commun. 391 (4), 1698-1702.

Jheng, G.W., Hur, S.S., Chang, C.M., Wu, C.C., Cheng, J.S., Lee, H.H., Chung, B.C., Wang, Y.K., Lin, K.H., Del Álamo, J.C., 2018. Biochem. Biophys. Res. Commun. 497 (3), 869-875.

Ju, L., Zhu, C., 2017. Biophys. J. 113 (12), 2842-2845.

Ju, L., Chen, Y., Li, K., Yuan, Z., Liu, B., Jackson, S.P., Zhu, C., 2017. Sci. Rep. 7 (1),

Juette, M.F., Terry, D.S., Wasserman, M.R., Zhou, Z., Altman, R.B., Zheng, O., Blanchard, S.C., 2014, Curr. Opin, Chem. Biol. 20, 103-111.

Julien, H., Karine, C., Armelle, B., Claire, H., Nelly, H., Agrewala, J.N., 2011. PloS One 6 (5), e19680.

Kai, F., Laklai, H., Weaver, V.M., 2016. Trends Cell Biol. 26 (7), 486-497.

Kobayashi, T., Sokabe, M., 2010. Cell Biol. 22, 669-676. Curr. Opin.

Kothapalli, D., Liu, S.L., Bae, Y.H., Monslow, J., Xu, T., Hawthorne, E.A., Byfield, F.J., Castagnino, P., Rao, S., Rader, D.J., 2012. Cell Rep. 2 (5), 1259-1271.

Aird, E.J., Tompkins, K.J., Ramirez, M.P., Gordon, W.R., 2020. ACS Sens. 5 (1), 34-39. Ashkin, A., Schutze, K., Dziedzic, J.M., Euteneuer, U., Schliwa, M., 1990. Nature 348 (6299), 346-348.

Ayala, Y.A., Pontes, B., Hissa, B., Monteiro, A.C.M., Farina, M., Moura-Neto, V., Viana, N. B., Nussenzveig, H.M., 2017. Exp. Cell Res. 351 (2), 173-181.

Banda, O.A., Sabanayagam, C.R., Slater, J.H., 2019. ACS Appl. Mater. Interfaces 11 (20), 18233-18241.

Barsky, S.H., Rao, C.N., Grotendorst, G.R., Liotta, L.A., 1982. Am.j.pathol. 108 (3), 276-283.

- Kroemer, G., Senovilla, L., Galluzzi, L., André, F., Zitvogel, L., 2015. Nat. Med. 21 (10), 1128–1138.
- Lang, N.R., Skodzek, K., Hurst, S., Mainka, A., Steinwachs, J., Schneider, J., Aifantis, K. E., Fabry, B., 2015. Acta Biomater. 13, 61–67.
- Legant, W.R., Choi, C.K., Miller, J.S., Shao, L., Gao, L., Betzig, E., Chen, C.S., 2013. Proc. Natl. Acad. Sci. U.S.A. 110 (3), 881–886.
- Levental, K.R., Yu, H., Kass, L., Lakins, J.N., Egeblad, M., Erler, J.T., Fong, S.F.T., Csiszar, K., Giaccia, A., Weninger, W., Yamauchi, M., Gasser, D.L., Weaver, V.M., 2009. J. Cell. 139 (5), 891–906, 2009.
- Li, M., Xiao, X., Liu, L., Xi, N., Wang, Y., Dong, Z., Zhang, W., 2013. Exp. Cell Res. 319 (18), 2812–2821.
- Li, M., Dang, D., Xi, N., Wang, Y., Liu, L., 2017a. Nanoscale 9 (45), 17643–17666.
- Li, M., Dang, D., Liu, L., Xi, N., Wang, Y., 2017b. IEEE T Nanobiosci 16 (6), 523–540.
- Li, I.T.S., Chemla, Y.R., Ha, T., 2017c. Biophys. J. 112 (3), 1(a).
- Li, F., Chen, A., Reeser, A., Wang, Y., Fan, Y., Liu, S., Zhao, X., Prakash, R., Kota, D., Li, B., Yokota, H., Liu, J., 2019. Sci. Rep. 9 (1), 5615.
- Li, C.Y., Zhang, T., Kang, Y.F., Qi, C.B., Zheng, B., Xu, C.M., Lin, Y., Pang, D.W., Tang, H. W., 2020. Chem. Commun. 56 (51), 6997–7000.
- Liu, Z., Tan, J.L., Cohen, D.M., Yang, M.T., Sniadecki, N.J., Ruiz, S.A., Nelson, C.M., Chen, C.S., 2010. Proc. Natl. Acad. Sci. U.S.A. 107 (22), 9944–9949.
- Liu, Y., Yehl, K., Narui, Y., Salaita, K., 2013. J. Am. Chem. Soc. 135 (14), 5320–5323.
- Liu, B., Chen, W., Evavold, B.D., Zhu, C., 2014. Cell. Mol. Bioeng. 157 (2), 357-368.
- Liu, Y., Blanchfield, L., Ma, V.P., Andargachew, R., Galior, K., Liu, Z., Evavold, B.D., Salaita, K., 2016. Proc. Natl. Acad. Sci. U.S.A. 113 (20), 5610–5615.
- Liu, Y., Galior, K., Ma, V.P., Salaita, K., 2017. Acc. Chem. Res. 50 (12), 2915–2924. Lu, P., Takai, K., Weaver, V.M., Werb, Z., 2011. Cold Spring Harb. Perspect. Biol. 3 (12)
- a005058–a005058. Luca, V.C., Kim, B.C., Ge, C., Kakuda, S., Wu, D., Roein-Peikar, M., Haltiwanger, R.S.,
- Zhu, C., Ha, T., Garcia, K.C., 2017. Science 355 (6331), 1320–1324. Ma, V.P., Salaita, K., 2019. Small 15 (26), 1900961.
- Ma, P.Y., Liu, Y., Yehl, K., Galior, K., Zhang, Y., 2016. Angew. Chem., Int. Ed. Engl. 128 (18), 5578–5582.
- Ma, R., Kellner, A.V., Ma, P.Y., Su, H., Salaita, K., 2019. Proc. Natl. Acad. Sci. U. S. A 116 (34), 16949–16954.
- Mammoto, T., Jiang, E., Jiang, A., Mammoto, A., 2013. Am. J. Respir. Cell Mol. Biol. 49 (6).
- Mandal, K., Asnacios, A., Goud, B., Manneville, J., 2016. Proc. Natl. Acad. Sci. U.S.A. 113 (46), 201605112.
- Maruthamuthu, V., Sabass, B., Schwarz, U.S., Gardel, M.L., 2011. Proc. Natl. Acad. Sci. U. S.A. 108 (12), 4708–4713.
- Matthews, B.D., Overby, D.R., Mannix, R., Ingber, D.E., 2006. Cell Sci 119 (3), 508–518. McDaniel, S.M., Rumer, K.K., Biroc, S.L., Metz, R.P., Singh, M., Porter, W., Schedin, P., 2006. Am. J. Pathol. 168 (2), 608–620.
- Mckenzie, A.J., Hicks, S.R., Svec, K.V., Naughton, H., Edmunds, Z.E.L., Howe, A.K., 2018. Sci. Rep. 8 (1), 7228.
- Miroshnikova, Y.A., Jorgens, D.M., Spirio, L., Auer, M., Sarang-Sieminski, A.L., Weaver, V.M., 2011. Phys. Biol. 8 (2), 026013.
- Nawaz, S., Sanchez, P., Bodensiek, K., Li, S., Simons, M., Schaap, I.A.T., 2012. PloS One 7 (9), 45297.
- Neuman, C.K., Nagy, A., 2008. Nat. Methods 5 (6), 491–505.
- Paszek, M.J., Zahir, N., Johnson, K.R., Lakins, J.N., Rozenberg, G.I., Gefen, A., Weaver. V.M.. 2005. Canc. Cell 8 (5), 241–254.
- Pathak, A., Kumar, S., 2012. Proc. Natl. Acad. Sci. U.S.A. 109 (26), 10334-10339.

- Pinto, V.I., Senini, V.W., Wang, Y.Q., Kazembe, M.P., McCulloch, C.A., 2014. Faseb. J. 28 (1), 453–463.
- Polacheck, W.J., Chen, C.S., 2016. Nat. Methods 13 (5), 415-423.
- Puech, P.H., Poole, K., Knebel, D., Muller, D.J., 2006. Ultramicroscopy 106 (8–9), 637–644.
- Rabodzey, A., Alcaide, P., Luscinskas, F.W., Ladoux, B., 2008. Biophys. J. 95 (3), 1428–1438.
- Rathod, M.L., Pareek, N., Agrawal, S.S., Jaddivada, S., Lee, D.W., Gundiah, N., 2017. RSC Adv. 7 (81), 51436–51443.
- Rauskolb, C., Sun, S., Sun, G., Pan, Y., Irvine, K.D., 2014. Cell 158 (1), 143–156. Reilly, G.C., Engler, A.J., 2010. Biomech 43 (1), 55–62.
- Ronnov-Jessen, P.O.W., Bissell, M.J., 1996. Physiol. Rev. 76 (1), 69-125.
- Ruashkin, M.G., Cassereau, L., Bainer, R., DuFort, C.C., Yui, Y., Ou, G., Paszek, M.J., Davidson, M.W., Chen, Y.Y., Weaver, V.M., 2014. Canc. Res. 74 (7), 4597–4611.
- Sabass, B., Gardel, M.L., Waterman, C.M., Schwarz, U.S., 2008. Biophys. J. 94 (1), 207–220.
- Sancho, A., Vandersmissen, I., Craps, S., Luttun, A., Groll, J., 2017. Sci. Rep. 7, 46152. Schoen, I., Hu, W., Klotzsch, E., Vogel, V., 2010. Nano Lett. 10 (5), 1823–1830.
- Schwingel, M., Bastmeyer, M., 2013. PloS One 8 (1), e54850, 2013. Septiadi, D., Crippa, F., Moore, T., Rothenrutishauser, B., Petrifink, A., 2018. Adv. Mater.
- Sepidad, D., Crippa, F., Moore, T., Romeirdushauser, B., Petrinik, A., 2018. Adv. Mater. Interfaces. 30 (19), 1704463. Shi, R., Cui, H., Bi, Y., Huang, X., Song, B., Cheng, C., Zhang, L., Liu, J., He, C., Wang, F.,
- 2015. Oncol. Lett. 9 (5), 2249. Sickafoose, L.K., Chen, Q.J., Wood, M.B., Cardiff, R.D., Gregg, J.P., Borowsky, A.D.,
- Sickatoose, L.K., Chen, Q.J., Wood, M.B., Cardiff, R.D., Gregg, J.P., Borowsky, A.D., 2006. Canc. Res. 66, 418–419.
- Stabley, D.R., Jurchenko, C., Marshall, S.S., Salaita, K.S., 2012. Nat. Methods 9 (1), 64–67.
- Stone, J., Dite, G.S., Gunasekara, A., English, D.R., McCredie, M.R.E., Giles, G.G., Cawson, J.N., Hegele, R.A., Chiarelli, A.M., Yaffe, M.J., Boyd, N.F., Hopper, J.L., 2006. Cancer epidemiol. Biomarkers Prev 15 (4), 612–617.
- Stylianou, A., Lekka, M., Stylianopoulos, T., 2018. Nanoscale 10 (45), 20930–20945. Touhami, A., Jericho, M.H., Beveridge, T.J., 2004. J. Bacteriol. 186 (11), 3286.
- Trepat, X.; Wasserman, M. R.; Angelini, T. E.; Millet, E.; Weitz, D. A.; Butler, J. P.; Fredberg, J. J., Nat. Phys. 5(6), 426-430.
- Tseng, P., Judy, J.W., Carlo, D.D., 2012. Nat. Methods 9 (11), 1113-1119.
- Wang, X., Ha, T., 2013. Science 340 (6135), 991-994.
- Wang, Y., Wang, X., 2016. Sci. Rep. 6, 36959.
- Wang, N., Butler, J.P., Ingber, D.E., 1993. Science 260 (5111), 1124-1127.
- Wang, X., Rahil, Z., Li, I.T.S., Chowdhury, F., Leckband, D.E., Chemla, Y.R., Ha, T., 2016.
 Sci. Rep. 6, 21584.
- Watson, C.J., 2006. Expet Rev. Mol. Med. 8 (32), 1-15.
- Wolf, K., Lindert, M., Krause, M., Alexander, S., Riet, J., Willis, A.L., Hoffman, R.M., Figdor, C.G., Weiss, S.J., Friedl, P., 2013. J. Cell Biol. 201 (7), 1069–1084.
- Xiao, L.F., Chen, Q., Wu, Y.Z., Qi, X.J., Zhou, A.H., 2015. BBA Biomembranes 1848 (10), 1988–1995.
- Yamashita, S., Tsuboi, T., Ishinabe, N., Kitaguchi, T., Michiue, T., 2016. Sci. Rep. 6 (1), 28535.
- Yan, C., Moutin, E., Hemonnot, A.L., Perroy, J., 2017. Front. Comput. Neurosci. 11, 118. Yin, Y., Zhao, X.S., 2011. Acc. Chem. Res. 44 (11), 1172–1181.
- Young, T.J., Monclus, M.A., Burnett, T.L., Broughton, W.R., Ogin, S.L., Smith, P.A., 2011.
 Meas. Sci. Technol. 22 (12), 125703.
- Zhang, Y., Ge, C., Zhu, C., Salaita, K., 2014. Nat. Commun. 5 (1), 5167-5167.
- Zohar, H., Hetherington, C.L., Bustamante, C.J., Muller, S.J., 2010. Nano Lett. 10 (11), 4697–4701.